Low temperature rolling of AZ91 alloy for hydrogen storage

Article *in* International Journal of Hydrogen Energy · November 2017

DOI: 10.1016/j.ijhydene.2017.10.035

INTERNATIONAL JOURNAL OF HYDROGEN ENERGY XXX (2017) 1–12

Available online at www.sciencedirect.com

ScienceDirect

journal homepage: www.elsevier.com/locate/he

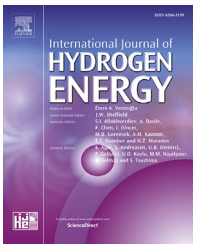

Low temperature rolling of AZ91 alloy for hydrogen storage

R. Floriano [a,*], D.R. Leiva [b], G.C. Melo [b], T.T. Ishikawa [b], J. Huot [c], M. Kaufman [d], S.J.A. Figueroa [e], L.A. Mendoza-Zélis [f], L.C. Damonte [f], W.J. Botta [b]

[a] Faculdade de Ciências Aplicadas, Universidade Estadual de Campinas, Rua Pedro Zaccaria, 1300, CEP 13484-350, Limeira, SP, Brazil

[b] Departamento de Engenharia de Materiais (DEMA), Universidade Federal de São Carlos, Rod. Washington Luiz, Km 235, 13565-905 São Carlos, SP, Brazil

[c] Institut de Recherche sur L'Hydrogène, Université Du Québec à Trois-Rivières 3351, Boulevard des Forges, C.P. 500, Trois-Rivières, Québec G9A 5H7, Canada

[d] Department of Metallurgical and Materials Engineering, Colorado School of Mines, 1500 Illinois Street, Golden, CO, USA

[e] Laboratório Nacional de Luz Síncrotron, Centro Nacional de Pesquisa Em Energia e Materiais, Rua Giuseppe Maximo Scolfaro, 10000, Caixa Postal 6192, CEP 13083-970, Campinas, SP, Brazil

[f] IFLP, Departamento de Física, Facultad de Ciencias Exactas, Universidad Nacional de La Plata, CC67, 1900 La Plata, Argentina

ARTICLE INFO

Article history:
Received 31 July 2017
Received in revised form
4 October 2017
Accepted 6 October 2017
Available online xxx

Keywords:
AZ91 alloy
Low temperature rolling
Severe plastic deformation
Hydrogen storage

ABSTRACT

The hydrogen storage properties of a commercial AZ91 magnesium alloy were investigated after processing by cold rolling in two different conditions: (a) extensive cold rolling at room temperature (CR); (b) rolling with the immersion of the alloy in liquid nitrogen bath after 05 rolling passes. This second condition is named as low temperature rolling (LTR). A full microstructural characterization including scanning and transmission electron microscopy (SEM and TEM), X-ray diffraction (XRD), X-ray photoelectron and positron annihilation life time spectroscopy (XPS and PALS) were performed in the processed alloys. The hydrogen storage properties were measured using a Sievert-type apparatus. The AZ91-alloy is composed by the β-Mg and $Mg_{17}Al_{12}$ phases, and after processing by CR, an intense peak broadening and strong [002] texture were observed in the alloys. The LTR processing resulted in a more fragile material containing more microcracks and exposed interfaces than the conventionally cold rolled one. The LTR sample also presented a more refined microstructure in comparison with CR sample. These features resulted in superior hydrogen storage properties for the LTR sample in comparison with the CR sample. In addition, the effect of surface contamination was also studied in detail and it was found to play a significant role during the activation kinetics.

* *Corresponding author.*
E-mail addresses: ricardo.floriano@fca.unicamp.br (R. Floriano), daniel.leiva@ufscar.br (D.R. Leiva), gucomelo@gmail.com (G.C. Melo), ishikawa@ufscar.br (T.T. Ishikawa), jacques.huot@uqtr.ca (J. Huot), mkaufman@mines.ed (M. Kaufman), santiago.figueroa@lnls.br (S.J.A. Figueroa), mendoza@fisica.unlp.edu.ar (L.A. Mendoza-Zélis), damonte@fisica.unlp.edu.ar (L.C. Damonte), wjbotta@ufscar.br (W.J. Botta).

https://doi.org/10.1016/j.ijhydene.2017.10.035

introduction

MgH_2 is a very interesting material for hydrogen storage applications, since it has very high gravimetric hydrogen capacity (7.6 wt%) and presents high reversibility and cyclability [1,2]. Besides, magnesium is a low cost and non-toxic metal and can be easily recycled. These features are very important to promote the wide application of hydrogen solid tanks [3].

Conventional (microcrystalline) MgH_2 has slow hydrogen absorption and desorption kinetics even at temperatures as high as 400 °C [3,4]. However, it is well known that nanostructuring Mg/MgH_2 by high-energy ball milling (HEBM) has a very positive impact on its hydrogen storage properties, leading to faster kinetics at much lower temperatures [4,5]. Nanocrystalline MgH_2-based materials prepared by HEBM present high specific surface area, which favors faster kinetics of hydrogen reaction, but they are also highly susceptible to air contaminants as oxygen or moisture, and therefore they should be processed and handled under inert atmosphere [5].

On the other hand, different processing routes based on extensive plastic deformation techniques, such as, cold rolling (CR) [6–8] and cold forging [9,10], or severe plastic deformation (SPD) techniques, such as, equal-channel angular pressing (ECAP) [11–13] and high-pressure torsion (HPT) [14,15] are being explored to produce Mg-based materials suitable for hydrogen storage applications, combining acceptable hydrogen storage properties with better air resistance. The main advantages of using SPD techniques instead of HEBM are that they could be much simpler, cost effective and close to industry practice, since it is normally performed in air, requiring only a few minutes or even seconds to accomplish the processing.

Extensive CR of Mg – 2.5 at% Pd samples was first performed by Dufour and Huot [8]. The air-exposed laminated samples presented faster activation (first hydrogenation) and similar kinetics of hydrogen absorption and desorption when compared to a similar sample ball milled for 2 h, which revealed the potential of SPD processing for the production of hydrogen storage materials.

Amira et al. [16] studied the effects of cold rolling in AZ91 Magnesium alloys in as-cast and die-cast states for hydrogen storage purposes. They showed that after CR processing, the AZ91 alloy presented faster activation and absorption/desorption kinetics when compared to pure magnesium. These improvements were attributed to the alloying elements available into the AZ91 alloy accompanied by the high number of defects and the nanocrystalline structure reached by the processing route.

We have studied some combinations of SPD processing routes to process Mg-based alloys and composites, such as conventional cold rolling [6,9,17,18], cold rolling under inert atmosphere [6], forging, ECAP or HPT, including or not some further steps of ball milling [10,20–25], and melt-spinning followed by CR [26,27]. These processing routes have resulted in very refined microstructures with interesting morphological aspects such as higher proportion of exposed interfaces and microcracks as well as the desired texture for hydrogenation. These microstructural aspects greatly enhanced the activation kinetics and the hydrogen storage properties in general. Regarding to the cold rolling, it has also been shown the positive effect to incorporate selected additives to MgH_2.

All the results cited so far [6–18,20–27] involving the SPD techniques deal with the processing of commercial Mg alloys for H-storage purposes under room temperature (e.g.: cold rolling, forging) and in some cases with relatively higher temperatures (e.g. ECAP). It is well known that the initial coarse microstructure can be a limiting factor to the grain refinement of Mg alloys, being necessary the use of different strategies to overcome this limitation [13–15].

Furthermore, concerning hydrogen storage properties, it has been already established the positive effect of alloying elements dispersed over the Mg matrix in comparison with pure Mg, the importance of a refined microstructure (preferably nanostructured), the presence of ultra fine grained materials, controlled texture, and also the increase in the specific surface area (surface/volume ratio) by generating more interfaces [8,11,15,25,28–30].

In this context, we suggest that the effect of cryogenic temperature associated with SPD processing of Mg alloys could be a potential tool to reach fine particle sizes and small recrystallized grain sizes in Mg alloys when compared to the same technique performed at room temperature. We also suggest to be relevant the use of techniques that can give information about defects distribution in mechanically processed alloys, such as positron annihilation lifetime spectroscopy (PALS). PALS is a powerful method to study open volume defects in solids [31], and it has been extensively used for the study of vacancies, clusters, kinetics and precipitations in Mg-based alloys [32–35]. Due to its high sensitivity, positron annihilation can give information on size and concentration of vacancy defects and their evolution during aging process of alloys. In particular, it has been applied to study the formation of precipitates in thermal aged AZ91 alloys [34,35].

The aim of this work is to evaluate the cryogenic temperature factor during processing, the final structure and hydrogen storage properties of a commercial AZ91-Mg alloy. We choose the extensive CR as a processing route, which has provided interesting results concerning the hydrogen storage properties [6,9,17,18]. A comparison between cold rolled AZ91-Mg samples performed in two different conditions: at room temperature (CR); and at low temperature (LTR), with the immersion of the sample into liquid nitrogen after 05 rolling passes are presented. In order to characterize the induced defects in the processed samples, PALS measurements were done.

Experimental

Samples preparation

Commercial Mg alloy (AZ91, with composition of 9% of Al, 1% of Zn, purchased from RIMA industrial) was used as starting material for the two processing conditions based on cold rolling: CR and CR. Disks of AZ91alloy with 1 mm of thickness and 30 mm of diameter were produced by machining. A commercial, duo reversible horizontal rolling mill (*FENN 55DC02-02AS*) operating in a frequency of 51 rpm, was used in this study.

Please cite this article in press as: Floriano R, et al., Low temperature rolling of AZ91 alloy for hydrogen storage, International Journal of Hydrogen Energy (2017), https://doi.org/10.1016/j.ijhydene.2017.10.035

For each rolling experiment, Mg-AZ91 disk was placed between two stainless steel plates to prevent the contamination with the rolls. After the first rolling pass, pieces or flakes of the fractured Mg disks were collected and inserted in the middle of the two plates and rolled again. This procedure was repeated up to 25 passes. For each rolling pass, the thickness reduction was estimated to be 50%.

For LTR processing, at first and after each five rolling passes, the sample was immersed in a liquid nitrogen bath for 5 min to reach the liquid nitrogen temperature, and then rolled again. Every rolling experiment was done under air atmosphere and the final product consisted of small flakes with around 0.1 mm thickness for both processing routes. The final products were stored in an argon filled glove-box (MBraun *Labmaster 1300 model*).

Fig. 1a–c show images of the Mg-AZ91 disk obtained by machining and after processing by CR and LTR, respectively. It should be pointed out the dark appearance of the sample processed by LTR in comparison to the CR sample. It occurred due to the water vapor condensation over the cold surface of metal, after immersion of the sample in liquid nitrogen.

Characterization techniques

AZ91samples were characterized by X-ray diffraction (XRD), using a Siemens D5005 diffractometer with monochromatic *CuKα* radiation ($\lambda = 1.5418$ Å) operating at 40 KV/40 mA. The XRD patterns were obtained in a 20° to 80° angular range (2θ) with a step size of 0.025° and counting time of 4 s/step.

The morphology and composition of the samples were examined by scanning electron microcopy (SEM) in a FEI Inspect S50 microscope coupled with energy dispersive spectroscopy (EDS). Microstructural details and the crystallite size evaluation were carried out in a FEI TECNAI G2 transmission electron microscopy (TEM).

Surface analyses were performed by X-ray Photoelectron Spectroscopy XPS, using a SPECSLAB II (Phoibos-Hsa 3500 150, 9 channeltrons) SPECS spectrometer, with monochromatic Al K-alpha radiation source (E = 1486.6 eV) operating at 1.5 kV, $E_{pass} = 40$, 0.5 eV energy step and acquisition time of 1.5 s per point.

In order to characterize the induced defects in the processed samples, Positron Annihilation Lifetime Spectroscopy (PALS) measurements were done. Spectra were collected in a conventional fast–fast coincidence system with two scintillator detectors (one BaF_2 and one plastic BURLE), which provided a time resolution (FWHM) of 280 ps. The radioactive source [22], NaCl (10 μCi), was deposited onto a kapton foil (1.42 g cm^{-3}) and sandwiched between two sample specimens. Source contribution and the response function were evaluated from a reference sample (Hf metal) using the RESOLUTION code [36]. The lifetime spectra ($2–3 \times 10^6$ counts) were acquired at room temperature and analyzed with the POSITRONFIT program [36].

Finally, the hydrogen storage properties were evaluated in a home-made Sieverts-type apparatus using samples with mass of around 150 mg. Absorption and desorption kinetic curves were measured at 623 K with hydrogen pressure of 2 MPa for absorption and 0.03 MPa for desorption.

Results

Typical microstructures of as-cast (ingot) AZ91 alloys are shown in http://www.sciencedirect.com/science/article/pii/S0925838812000977 Fig. 2. The back-scattered electrons (BSE) images show that the microstructure of as-cast AZ91 is composed of primary α-Mg as the matrix phase and the discontinuous and divorced $Mg_{17}Al_{12}$phase. The $Mg_{17}Al_{12}$-phase was confirmed by EDS analysis and it appears brighter in the SEM images.

The as-cast structure of α-Mg grains surrounded by coarse and reticular β-$Mg_{17}Al_{12}$ phase leads to the limited ductility during deformation [37]. The grain sizes of AZ91 casting products normally range between 10 μm and 150 μm [31,38]. The white particles areAl_8Mn_5 compound (γ-brass phase).

Fig. 3 shows a comparison between the XRD patterns for the AZ91 alloy in the following states: as-cast, CR and LTR. The same two phases were identified in all XRD patterns: Mg and $Mg_{17}Al_{12}$. The latter one is expected to be present in AZ91 alloys and was also confirmed by SEM analysis (Fig. 1).

It is also relevant to point out in Fig. 3 that there is a strong preferential orientation associated with the [0002] type texture in the Mg phase. As already reported in Refs. [20–25,39], crystallographic orientation along the (002) direction remarkably increases the hydrogen storage properties of Mg. In the study presented by Jorge Junior et al. [25] the positive influence of this crystallographic orientation in terms of capacity, kinetics and desorption temperature of pure Mg processed by ECAP and CR have been showed.

SEM images of AZ91 samples after cold rolling processing in the two different conditions are shown in Fig. 4. These images clearly reveal that as a result of the processing at low temperatures, the LTR sample has many more cracks and

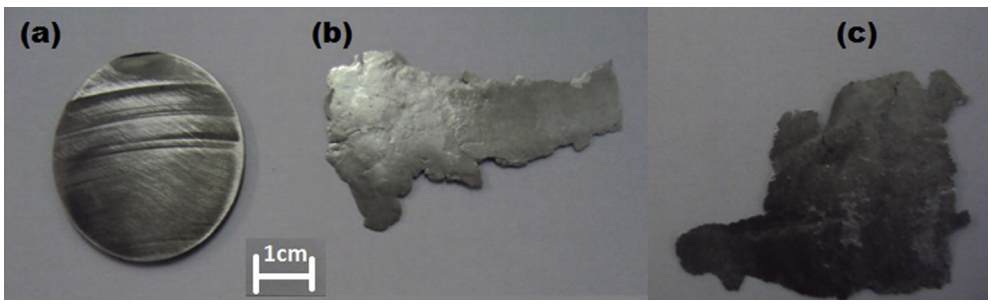

Fig. 1 – Images of Mg-AZ91 before (a) and after the CR (b) and LTR (c) processing conditions.

Please cite this article in press as: Floriano R, et al., Low temperature rolling of AZ91 alloy for hydrogen storage, International Journal of Hydrogen Energy (2017), https://doi.org/10.1016/j.ijhydene.2017.10.035

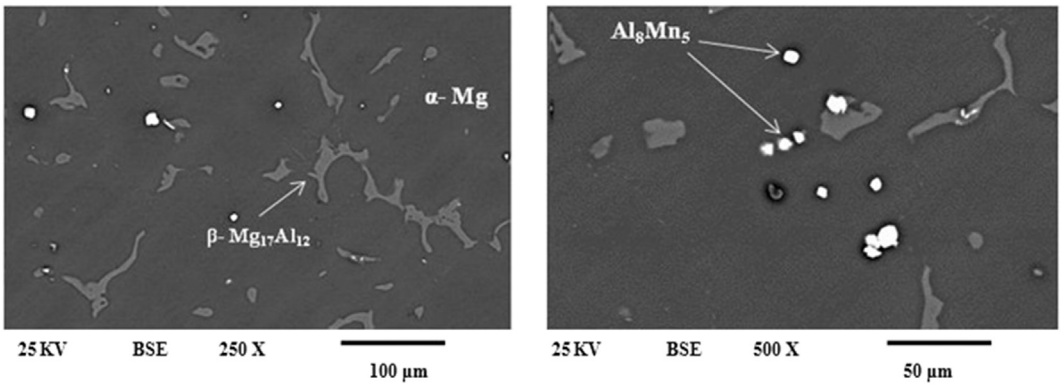

Fig. 2 – SEM images of as-cast AZ91 Mg alloy in BSE mode.

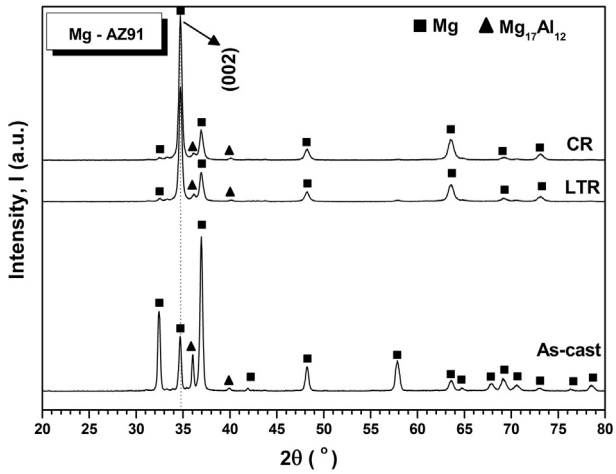

Fig. 3 – XRD patterns of the Mg-AZ91 samples in the conditions: as-cast, CR and LTR. The preferential orientation along the (002) direction is shown in detail.

fracture surfaces than the CR sample. In addition to the thermal shock of the sample during the immersion into liquid nitrogen bath before rolling, deformation at low temperatures decrease ductility and result in larger surface area associated with the several layers of cold welded flakes of magnesium with high amount of exposed interfaces in comparison with the CR sample.

Asselli et al. [29] showed that one of the key factors to improve the hydrogen storage properties of magnesium is to increase the surface/volume ratio of the material, leading to faster activation and enhanced hydrogen storage properties. In this case, the Mg was prepared by CR followed by filing.

TEM observations also indicated important differences in the microstructural features associated with the two processing routes proposed here.

Figs. 5 and 6 show representative TEM images of AZ91 samples after processing by cold rolling in the CR and LTR conditions, respectively. The selected area diffraction pattern (SADP) of the polycrystalline region in both samples (Figs. 5c and 6c.) clearly shows that all of the diffraction rings can be indexed according to Mg phase, which is consistent with the XRD results (Fig. 2).

The bright and dark field images (Figs. 5 and 6 (a) and(b)) show the formation of a heavily deformed microstructure, characterized by regions with high dislocation density with grains or subgrains in the nanometer range.

On the other hand, rolling at low temperature leads to the formation of a microstructure significantly more refined in comparison with the conventional rolling. From the TEM images, the CR sample shows a grain size of about 250 nm while for the LTR sample a grain size of 100 nm is observed. The grain size observed in the cold rolled sample can be compared with the ones published in Ref. [28] where a similar grain size was achieved by ECAP of ZK60 alloy. On the other hand, the grain size observed for the LTR sample is still smaller when compared to those results published in Refs. [22–27].

The formation of a more refined microstructure in the LTR sample is due to creation of higher density of defects and effective suppression of dynamic recovery during rolling at low temperature. The severe strain induced at very low temperature facilitates the formation and retention of high density of dislocations, which acts as a driving force for the formation of sub-structures followed by ultrafine grains.

As already reported in Refs. [11,15,30] plastic deformation increases the density of microstructural defects, such as dislocations and vacancies, which can intensify diffusion kinetics of hydrogen. Additionally, heavily deformed microstructures typically lead to refined grains creating more boundaries that serve as pathways for hydrogen.

Fig. 7 compares the activation kinetics (first absorption) curves at 623 K under2 MPa of hydrogen pressure for the AZ91 samples after CR and LTR processing conditions. The as-cast AZ91 sample did not present any hydrogen absorption after 40 h, and for this reason the corresponding curve is not shown here.

In Fig. 7, we can clearly see that, at the beginning, the CR sample showed activation kinetics faster than the LTR sample, but after approximately 24 h, the activation kinetics for the CR sample became faster than the one observed for the LTR sample. After 40 h, the hydrogen capacity measured is higher for LTR (6.5 wt% of H_2) sample in comparison with the CR sample (4 wt% of H_2). However, another interesting feature from these activation kinetics curves is the incubation time, which is much larger for the LTR sample (11 h) than for CR sample (6 h).

A detailed SEM investigation on the surface aspects of the AZ91 alloys after processing can indicate the reasons for the

Please cite this article in press as: Floriano R, et al., Low temperature rolling of AZ91 alloy for hydrogen storage, International Journal of Hydrogen Energy (2017), https://doi.org/10.1016/j.ijhydene.2017.10.035

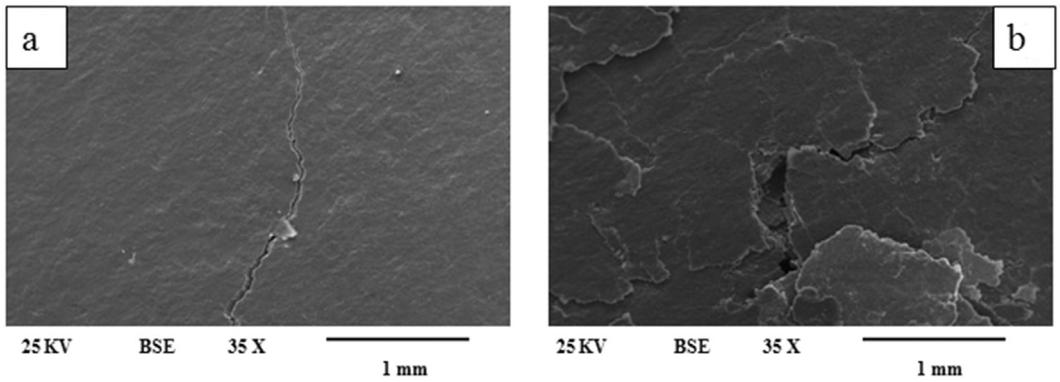

Fig. 4 – SEM images of AZ91 samples after cold rolling processing in the (a) CR and (b) LTR conditions.

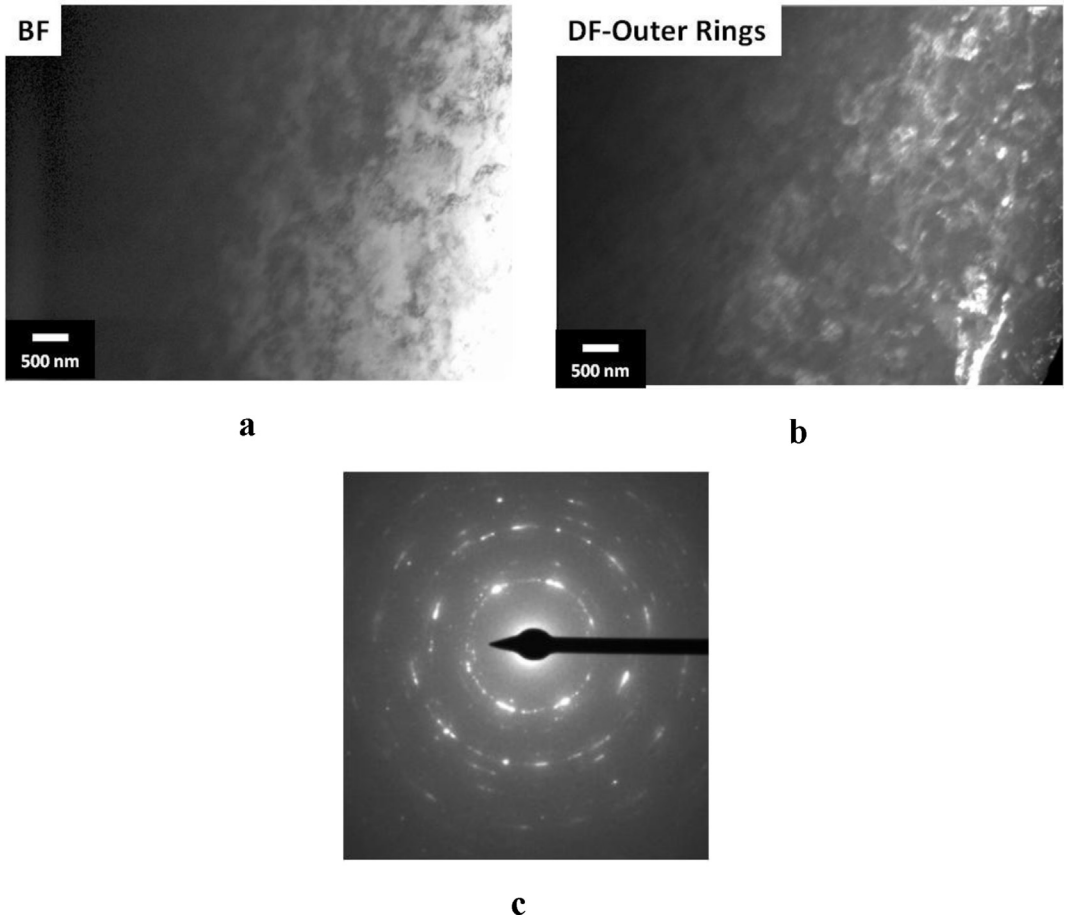

Fig. 5 – TEM images of cold rolled AZ91 sample. a) Bright field image; b) dark field image, c) SADP area.

observed differences in the activation and incubation times. Fig. 8 shows SEM images in the BSE mode for the AZ91 samples processed in the different conditions. Fig. 8(a) and (b) correspond to the CR sample and Fig. 8 (c) and (d) to the LTR sample. Both samples present in their surfaces dark regions distributed as a network with length around 200 μm. However, the LTR sample exhibits a higher concentration of dark regions in comparison with the CR sample. EDS analyses performed in the bright and dark regions (as indicated by points ***Ax*** and ***Bx*** in Fig. 8d for the LTR sample) resulted in the spectra shown in Fig. 8e. The quantification (wt%) of the elements Mg, Al, and O is included in this same Figure.

The EDS spectrum corresponding to the bright region (point ***Ax***) shows a Mg-based matrix composed by 87,4% of Mg, 9,5% of Al and 3,2% of O. On the other hand, the EDS spectrum corresponding to the dark region (point ***Bx***) indicated a much higher concentration of oxygen (39,1%), than measured in the bright phase (3,2%). The elemental mappings of Mg and O elements corresponding to Fig. 8d are shown at Fig. 8f and g, respectively. These maps clearly show that the dark regions

Please cite this article in press as: Floriano R, et al., Low temperature rolling of AZ91 alloy for hydrogen storage, International Journal of Hydrogen Energy (2017), https://doi.org/10.1016/j.ijhydene.2017.10.035

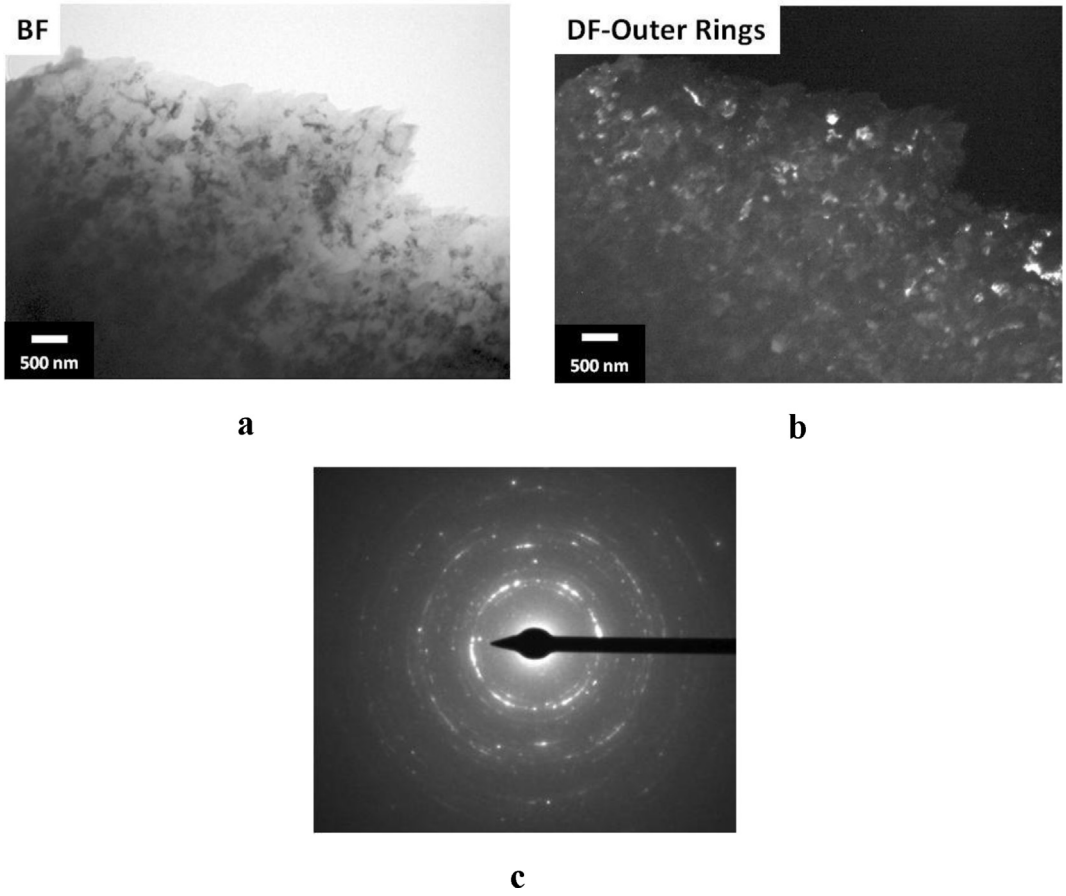

Fig. 6 – TEM images of cold rolled AZ91 sample at cryogenic temperature. a) Bright field image; b) dark field image, c) SADP area.

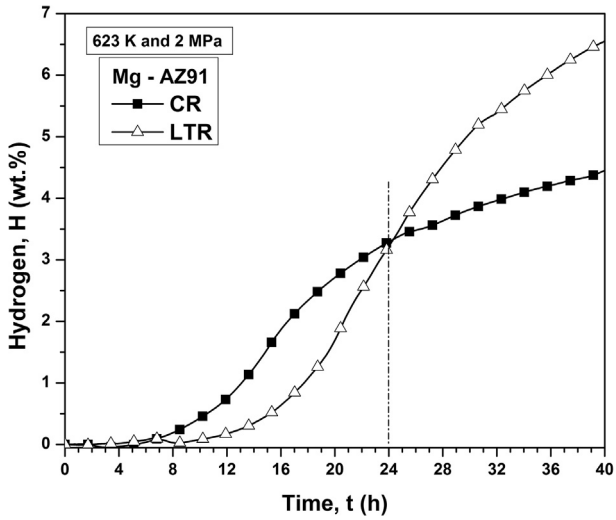

Fig. 7 – Activation kinetics curves for Mg-AZ91 samples after CR and LTR processing conditions.

are mostly composed of oxygen and this element can be associated to a contamination of magnesium oxide and/or hydroxide. The higher concentration of oxide/hydroxide in the LTR sample can be explained by the water vapor condensation over the cold surface of metal, which occurs after the nitrogen liquid bath in the sample during the rolling at low temperature.

The presence of magnesium oxide/hydroxide over the Mg surface is well known to cause degradation of the absorption and desorption hydrogen kinetics [6–8]. XPS technique was then used to estimate the amount of contaminants and also to identify the nature of these oxides present in the surface of processed samples [40–42].

Fig. 9 (a) and (b) show, respectively, the Mg-2p composite peak for CR and LTR samples. The three main contributions which are observed correspond to metallic Mg, MgO/$Mg(OH)_2$ and $MgCO_3$. The peak around 49.6 eV is associated with Mg in metallic state, and since the electrons had to penetrated the surface oxide layer, the presence of this peak suggest particularly thin oxide layer. The broad peak around 52.0 eV after correction for charging correspond to the mixture MgO/$Mg(OH)_2$. There was also a peak attributed to magnesium present in $MgCO_3$ in some cases around 53 eV. This latter one is more pronounced in the LTR sample than in CR sample. The fitting parameters for both samples are fully reported in Table 1. The presence of $MgCO_3$ could be understood through the combination of water condensation in the surface (after the immersion in liquid nitrogen bath) in contact with CO_2 in the air may lead the formation of H_2CO_3. At lower temperatures, this latter one can react with Mg metallic forming $MgCO_3$. A quantitative XPS study of the surface films formed by

Please cite this article in press as: Floriano R, et al., Low temperature rolling of AZ91 alloy for hydrogen storage, International Journal of Hydrogen Energy (2017), https://doi.org/10.1016/j.ijhydene.2017.10.035

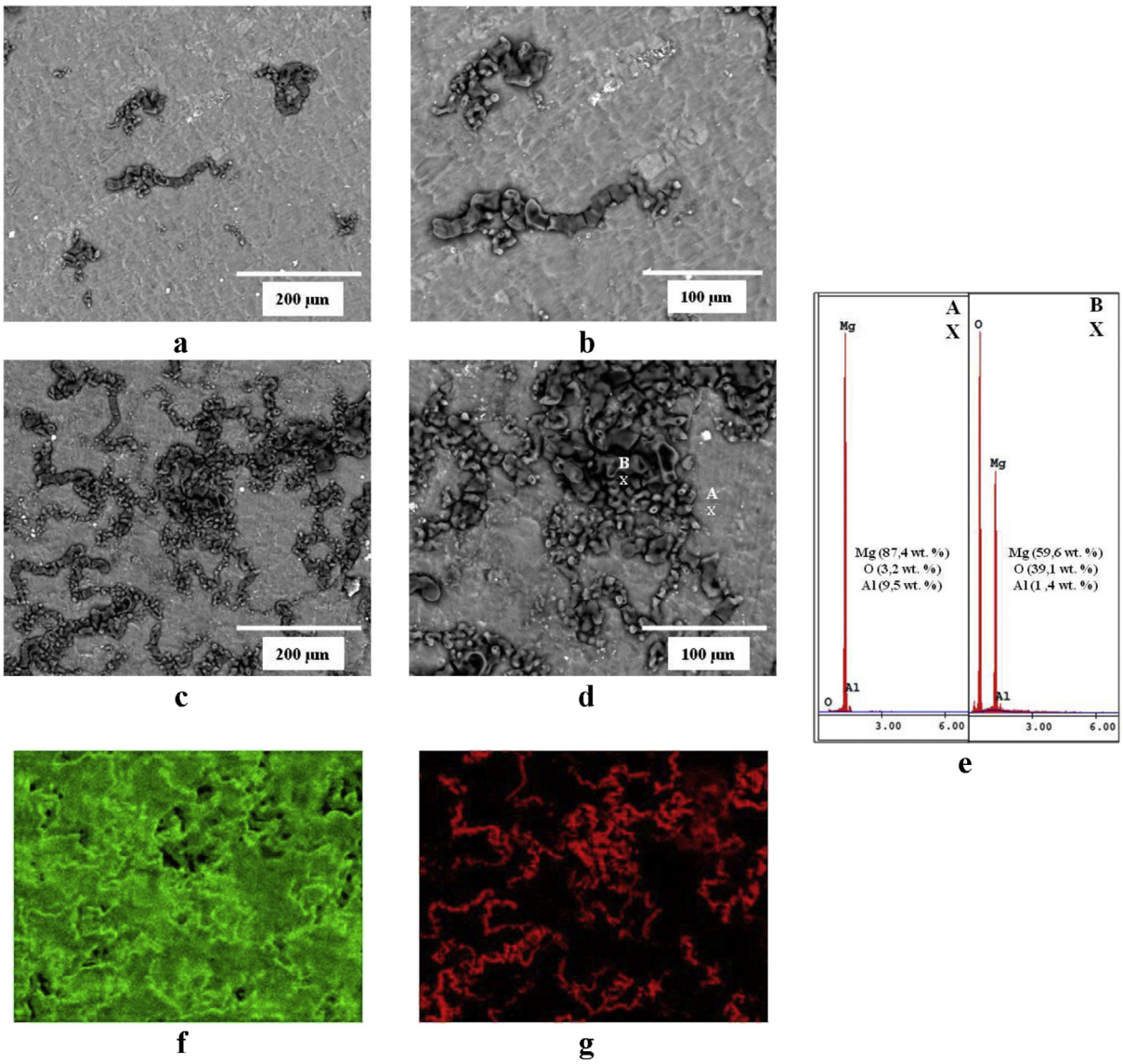

Fig. 8 – SEM images in BSE mode of AZ91 samples after conventional cold rolling (8a and 8b) and at cryogenic temperature (8c and 8d). e) EDS spectra taken from the points A and B of Fig. 8d. f), g) mapping of Mg and O from the image 8c.

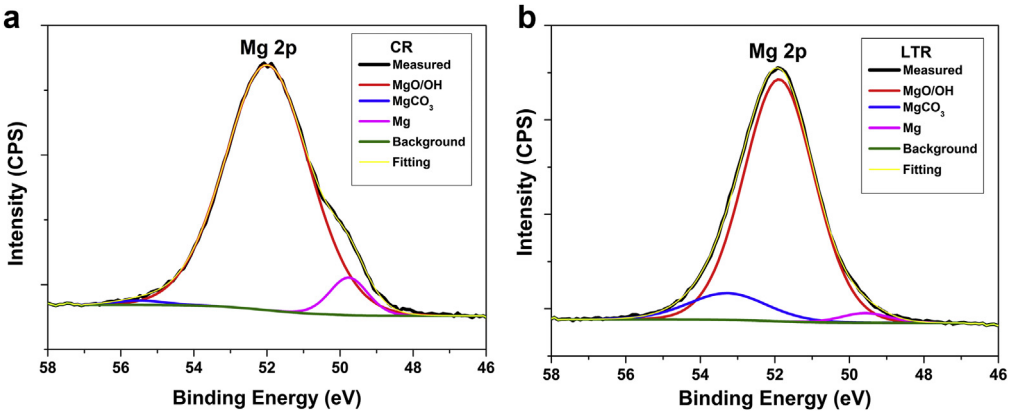

Fig. 9 – Peak deconvolution of the Mg 2p for a) CR and b) LTR samples.

Please cite this article in press as: Floriano R, et al., Low temperature rolling of AZ91 alloy for hydrogen storage, International Journal of Hydrogen Energy (2017), https://doi.org/10.1016/j.ijhydene.2017.10.035

exposure to water on Mg and on the Mg–Al intermetallics can be found in Ref. [41].

Since surface reactions certainly affect hydrogen sorption properties, the effect of surface cleaning on the hydrogen kinetics behavior, after CR and LTR processing was also investigated. The processed samples were then carefully polished using sandpaper and their hydrogen storage properties were again evaluated. Fig. 10 (a) shows the activation kinetics curves for the Mg-AZ91 CR and LTR samples after polishing the exposed surfaces. A dramatic enhancement in the incubation time was observed in the polished samples in comparison with the as-processed samples shown in Fig. 7.

In general, the activation kinetics become faster in both samples after polishing the surfaces with absorption starting immediately for the LTR sample without any incubation time, while for the CR sample a smaller incubation time of about 4 h was observed.

From these results, we can argue that the LTR sample is more reactive to the hydrogen reaction than the CR sample. The hydrogen capacity observed is around 5.6 wt% of H_2 for LTR sample against 3.1 wt% of H_2 for CR sample.

The effect of surface cleaning on the incubation time in LTR sample is shown in Fig. 10 (b). Fig. 10 (b) shows the activation kinetics curves before and after polishing the surfaces in LTR sample only. As we could see, the incubation time was significantly reduced from 11 h to almost zero with the sample starting to absorb immediately.

Fig. 11 compares desorption kinetics curves at 623 K under 0.1 MPa of hydrogen pressure for the Mg-AZ91 CR and LTR samples. The desorption kinetics is faster for the LTR sample in comparison with CR sample reaching a full desorption after 7200 s. In addition, almost complete desorption is observed only for the LTR.

The second absorption kinetics curves are shown in Fig. 12. Absorption is much faster at the beginning for the LTR sample, but after a few hours the curves have the same slope and therefore, the same kinetics. The main difference in these curves refers to the hydrogen capacity, which is higher for the LTR sample than for the CR sample (4 wt% of H_2 for LTR sample, and 1,5 wt% of H_2 for CR sample after 8 h).

Fig. 13 shows the second desorption kinetic curves at 623 K under 0.1 MPa for both samples. Again, the LTR sample presents faster desorption kinetics and full desorption after 6000 s, confirming the same trend observed in Fig. 11.

Fig. 14 compares the XRD patterns of the LTR and CR samples after cycling in the dehydrogenated state (second cycle). Some differences are clearly notable in these XRD patterns in comparison with XRD patterns shown at Fig. 2. Firstly, new diffraction peaks for the Mg and $Mg_{17}Al_{12}$ phases are now visible probably due to the new exposed interfaces after cycling. Secondly, the preferred orientation associated with the [0002] type texture for the Mg phase still remains in the patterns even after the cycling.

However, in the LTR sample, weaker texture is observed in comparison with the CR sample, which is probably associated to its complete hydrogenation. It is likely that the stronger remaining texture in the CR sample is due to the poor capacity to absorb hydrogen. This feature is observed in Figs. 10–13. It is also important to note that no traces of different phases were identified in these XRD patterns (Fig. 14).

In order to evaluate the size and concentration of vacancy defects in CR and LTR samples processed in different conditions, positron annihilation lifetime spectroscopy (PALS) was applied. PALS spectra, very similar for both samples, were decomposed into three exponential decays according to the following expression:

$$n(t) = \sum_i I_i \exp(-t/\tau_i)$$

being the relative intensities I_i, normalized, $\tau_i = 1$. After background subtraction and convolution with the resolution function, the parameters that characterized each positron state, τ_i, annihilation rate ($\tau_i = 1/\tau_i$) and its intensity I_i are obtained by means of POSITRONFIT program [36].

The resulting positron lifetime parameters are displayed in Table 2. Second (386 ps) and third lifetime (~1.6 ps) components described positron trapped in the source itself (kapton foil and adhesive), so they are not characteristic of the sample. Within the statistical error both analysis are quite similar. However, the corresponding intensity for τ_2 is rather high (I_2~25%) in order to account only source correction. So it might also include a slight contribution from some positron trapped at dislocations or grain boundaries [35]. The first component, τ_1, with values of 226 ps and 220 ps for RT and LTR samples are in agreement with previous positron annihilation studies [34,35].

This observed life time contains two or more unresolved components, which represents free positron annihilation in the sample, single vacancies or different phases. Bulk positron annihilation life time for Mg and Al are 225 ps and 216 ps, respectively.

Since AZ91 alloy consists of a mixture of α-Mg and β-$Mg_{17}Al_{12}$ phases, Ortega et al. [35] proposed a mathematical expression to obtain its characteristic positron annihilation lifetime, which yield a value of 218 ps. In consequence, the slight decrement of about 6–7 ps from RT to LTR state alloy might be due to an increase in β-$Mg_{17}Al_{12}$ phase concentration or a decrease in metallic Mg as it was observed by XPS (Table 1). In addition, the fact that I_2 remains constant for both states means that no new defects are induced by the LTR process.

Table 1 – Curve fitting parameters for Mg 2p.

Sample	Peak energy (eV)	Species	% Area under Curve
CR-RT	49.78	Mg metallic	7.05
	51.15	$MgO/Mg(OH)_2$	91.97
	54.52	$MgCO_3$	0.98
LTR	49.57	Mg metallic	2.34
	50.87	$MgO/Mg(OH)_2$	87.04
	52.26	$MgCO_3$	10.61

Discussion

In the present investigation, we evaluate in details the effect of low temperature (cryogenic temperature) during cold rolling of AZ91 samples. An initial characterization of AZ91 alloy in the as–received state performed by SEM and XRD

Please cite this article in press as: Floriano R, et al., Low temperature rolling of AZ91 alloy for hydrogen storage, International Journal of Hydrogen Energy (2017), https://doi.org/10.1016/j.ijhydene.2017.10.035

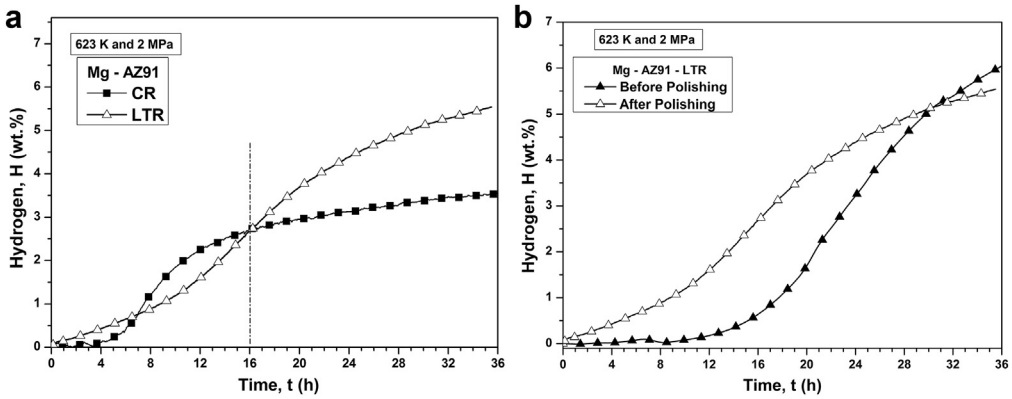

Fig. 10 – a) Activation kinetics curves for Mg-AZ91 samples after CR and LTR processing conditions after polishing the surfaces. b) Activation kinetics curves for LTR sample before and after polishing the surfaces.

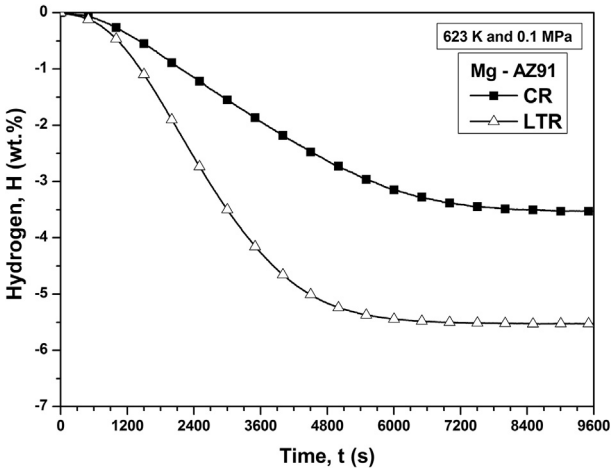

Fig. 11 – Desorption kinetics curves for Mg-AZ91 samples after CR and LTR processing conditions.

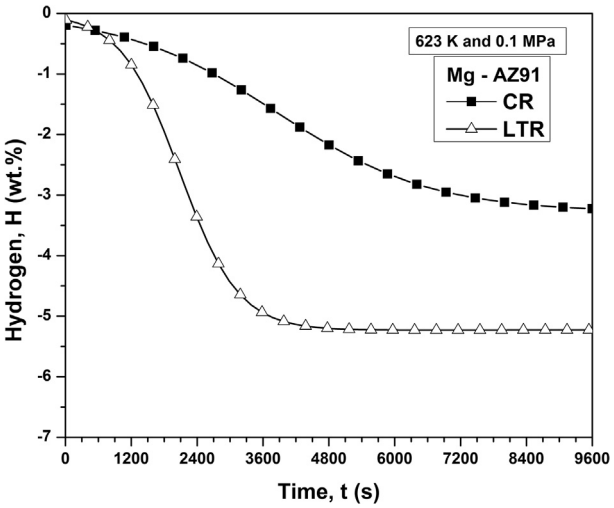

Fig. 13 – Desorption kinetics curves for Mg-AZ91 samples after CR and LTR processing conditions.

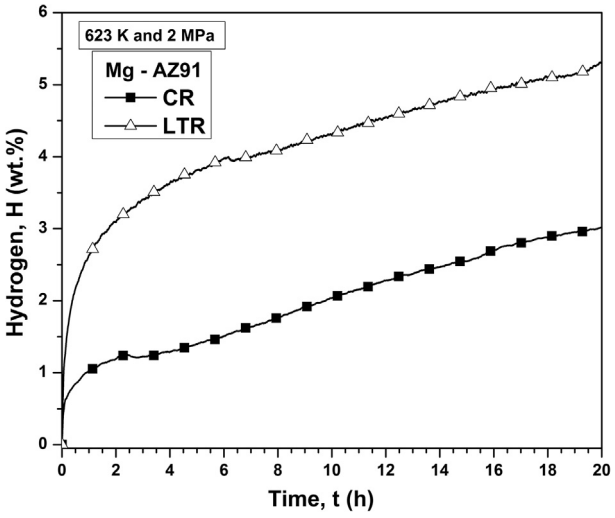

Fig. 12 – Absorption kinetics curves for Mg-AZ91 samples after CR and LTR processing conditions.

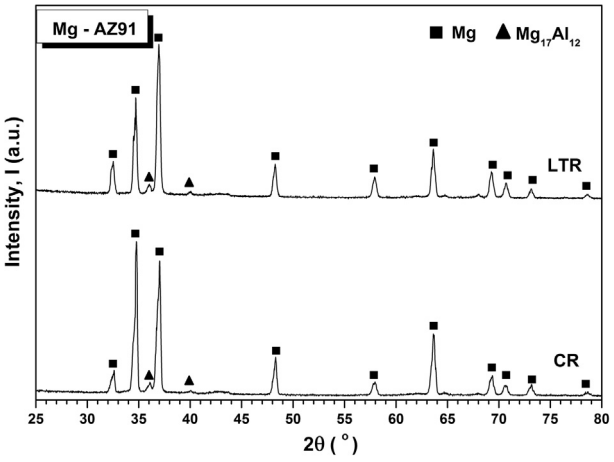

Fig. 14 – XRD patterns of Mg-AZ91 samples: CR and LTR after cycling (dehydrogenated state).

Please cite this article in press as: Floriano R, et al., Low temperature rolling of AZ91 alloy for hydrogen storage, International Journal of Hydrogen Energy (2017), https://doi.org/10.1016/j.ijhydene.2017.10.035

Table 2 – Positron annihilation parameters obtained from PATFIT analysis.

Sample	τ_1	I_1	τ_2	I_2	τ_3	I_3
RT	226_4	74_2	386	24_2	1688_{52}	2.8
LTR	220_4	73_1	386	25_1	1651_{51}	2.65

Underline means fixed parameter.

techniques shows that the matrix of AZ91 alloy consists of primary α-Mg phase and β-$Mg_{17}Al_{12}$ phase. The presence of β-$Mg_{17}Al_{12}$ particles can be related to the improvements in H-storage properties, since they may act as nucleation point for the hydride phase [16].

After rolling the samples in two different conditions (CR and LTR), the XRD patterns did not shown any significant difference in the processed samples, only a strong texture in [002] direction accompanied by the peak broadening of the Bragg peaks were well noticed. However, SEM images revealed a higher incidence of cracks (and also cold-welded layers) and exposed interfaces in the LTR sample in comparison with CR sample.

It is well known that microstructural refinement can enhance the kinetics of hydrogen absorption and desorption of magnesium-based materials [11,15,30]. This is because grain boundaries can act as nucleation sites for the hydride phase and also because hydrogen diffusion is generally faster along grain boundaries. With that, the TEM analysis of both samples reveals a large density of defects caused by the CR processing in both samples. However, a more pronounced microstructural refinement was observed for the LTR sample instead of CR sample. It was related to the effective suppression of dynamic recovery of AZ91 alloy during the immersion of sample in cryogenic liquid.

The grain sizes values observed are in the range of about 100 nm and 250 nm for LTR and CR samples, respectively. In a previous investigation [6] we showed that the effects of CR processing under inert atmosphere is a powerful tool for faster activation of pure Mg. With the cold rolling of Mg under air atmosphere, the material becomes much more reactive with the gradual reduction on particle size produced by the high deformation, turning more susceptible to contamination. The presence of contaminants such as oxides and hydroxides over the Mg surface contributes for a degradation of the hydrogen kinetics properties [6,43,44].

This effect/influence was very well evidenced in the activation kinetics curves measured before and after polishing the surfaces of processed samples. Before polishing, longer incubation times were observed in the samples and this feature was associated with the presence of the following contaminants found over the Mg surface: MgO, $Mg(OH)_2$ and $MgCO_3$. These contaminants were confirmed by the XPS together with EDS and SEM analysis. Furthermore, these techniques also revealed a high proportion of these contaminants in the LTR sample in comparison with CR sample. A reasonable explanation for that is due to the water vapor condensation over the cold surface of metal which occurs after the liquid nitrogen bath in the sample before the rolling pass. Also, in the LTR sample, a more refined microstructure is present, with higher amount of exposed interfaces and surface area. From the thermodynamical point of view, these regions are preferred sites for the formation of oxide/hydroxides.

After polished the surface of the samples, with subsequent extraction of the oxide and hydroxides layers as identified by XPS analysis, we could clearly see the beneficial effect of LTR. The kinetics results for the LTR sample are far superior than the corresponding results for CR sample. Faster activation, absorption and desorption kinetics are observed for the LTR sample in contrast with CR sample. Also, a more complete absorption and desorption kinetics process were features observed for the LTR sample in comparison with CR sample.

Finally, the CR processing at low temperature of AZ91 alloys resulted in improved hydrogen storage properties. The strategy used here based on the immersion of the AZ91 sample in the liquid nitrogen bath before and immediately after a certain number of rolling passes turns the sample more brittle to the subsequent deformation. This extreme brittleness results in a significant propagation of cracks and high volume/surface ratio of the material. These features are responsible for better hydrogen storage behavior observed in AZ91 alloy for LTR sample.

However, PALS measurements reveal an interesting finding regarding to the density of defects for the samples processed in both conditions; a similar density of defects was observed in both samples. Since a similar number of passes were employed in both samples, it could be related to the saturation of defects attained in the microstructure after the extensive rolling. Therefore, after the saturation of defects is attained in both samples, the subsequent rolling passes performed in LTR sample will play a significant role in comparison with the CR sample. As the LTR sample has more facility to break into small pieces due to the fragile behavior proportioned by the liquid nitrogen bath, more interfaces are created accompanied to a more refined microstructure in comparison with CR sample.

Conclusions

Mg-AZ91 alloy was processed by cold rolling in two different states: conventional cold rolling (CR) and with the immersion of the sample in the liquid nitrogen bath between the rolling passes (LTR). The main conclusions of this study are:

- The samples produced by rolling at low temperature have much better hydrogen sorption/desorption kinetics and capacity in comparison with the conventional cold rolling performed at room temperature, presenting faster kinetics and full absorption and desorption. The presence of microcracks and high amount of exposed interfaces in the LTR sample justify the good kinetics properties. The contaminant layer over the surface samples plays a significant role during the activation process, especially in the incubation time, which becomes shorter after grinding the samples.
- TEM analysis revealed the presence of a more refined microstructure for LTR sample than for RT sample as a result of deformation at low temperature.
- SEM and XPS analysis confirmed the presence of the major contaminants in the surface of samples after CR

Please cite this article in press as: Floriano R, et al., Low temperature rolling of AZ91 alloy for hydrogen storage, International Journal of Hydrogen Energy (2017), https://doi.org/10.1016/j.ijhydene.2017.10.035

processing, such as, $MgO/Mg(OH)_2$ and $MgCO_3$ (all of them in higher amount in the LTR sample)
- Strong preferred orientation of [0002] type texture was observed for the Mg phase after CR for both samples, which is also favorable to promote fast activation kinetics.
- Larger amount of cracks, cold welded layers formed in the LTR sample, resulting in larger surface area compared to the CR sample. These features are associated with the improved kinetics properties.

Further studies regarding the low temperature rolling are needed. Especially, the influence of the immersion of the sample after each rolling pass and the use of different Mg-alloys must be investigated.

Acknowledgements

The authors wish to thank São Paulo Research Foundation (FAPESP) (grant#2013/05987-8) and CNPQ (401429/2016-4) by the financial support.

REFERENCES

[1] Saba N, Taniya M, Altaf HP. Hydrogen storage: materials, methods and perspectives. Renew Sustain Energy Rev 2015;50:457–69.
[2] Wang H, Lin HJ, Cai WT, Ouyang LZ, Zhu M. Tuning kinetics and thermodynamics of hydrogen storage in light metal element based systems – a review of recent progress. J Alloys Compd 2016;658:280–300.
[3] Jehan M, Fruchart D. McPhy-Energy's proposal for solid state hydrogen storage materials and systems. J Alloys Compd November 2013;580:S343–8.
[4] Robert D. Stephens. Activation of metal hydrides. US Patent 2010; 7,700,069.
[5] De Castro JFR, Santos SF, Costa ALM, Yavari AR, Botta WJ, Ishikawa TT. Structural characterization and dehydrogenation behavior of Mg–5 at% Nb nano-composite processed by reactive milling. J Alloys Compds 2004;376:251–6.
[6] Floriano R, Leiva DR, Carvalho JA, Ishikawa TT, Botta WJ. Cold rolling under inert atmosphere: a powerful tool for Mg activation. Int J Hydrogen Energy 2014;39:4959–65. https://doi.org/10.1016/j.ijhydene.2014.01.070.
[7] Lang J, Huot J. A new approach to the processing of metal hydrides. J Alloys Compds 2011;509:L18–22.
[8] Dufour J, Huot J. Rapid activation, enhanced hydrogen sorption kinetics and air resistance in laminated Mg–Pd 2.5 at%. J Alloys Compd 2007;439:L5–7.
[9] Leiva DR, Floriano R, Huot J, Jorge AM, Bolfarini C, Kiminami CS, et al. Nanostructured MgH_2 prepared by cold rolling and cold forging. J Alloys Compds 2011;509S:444–8.
[10] Asselli AAC, Leiva DR, Cozentino GH, Floriano R, Huot J, Ishikawa TT, et al. Hydrogen storage properties of MgH_2 processed by cold forging. J Alloys Compd 2014;615(Suppl. 1):S719–24. https://doi.org/10.1016/j.jallcom.2014.01.065. ISSN 0925-8388, http://www.sciencedirect.com/science/article/pii/S0925838814000966.
[11] Krystian M, Zehetbauer MJ, Kropik H, Mingler B, Krexner G. Hydrogen storage properties of bulk nanostructured ZK60 Mg alloy processed by equal channel angular pressing. J Alloys Compd 2011;509:S449–55.
[12] Skripnyuk V, Buchman E, Rabkin E, Estrin Y, Popov M, Jorgensen S. The effect of equal channel angular pressing on hydrogen storage properties of a eutectic Mg–Ni alloy. J Alloys Compds 2007;436:99–106.
[13] Skripnyuk VM, Rabkin E, Estrin Y, Lapovok R. Improving hydrogen storage properties of magnesium based alloys by equal channel angular pressing. Int J Hydrogen Energy 2009;34:6320–4.
[14] Kusadome Y, Ikeda K, Nakamori Y, Orimo S, Horita Z. Hydrogen storage capability of $MgNi_2$ processed by high pressure torsion. Scr Mater 2007;57:751–3.
[15] Edalati K, Yamamoto A, Horita Z, Ishihara T. High-pressure torsion of pure magnesium: evolution of mechanical properties, microstructures and hydrogen storage capacity with equivalent strain. Scr Mater 2011;6:880–3.
[16] Amira S, Huot J. Effect of cold rolling on hydrogen sorption properties of die-cast and as-cast magnesium alloys. J Alloys Compds 2012;520:287–94.
[17] Floriano R, Leiva DR, Deledda S, Hauback BC, Botta WJ. Nanostructured MgH_2 obtained by cold rolling combined with short-time high-energy ball milling. Mater Res 2013;16(1):158–63.
[18] Floriano R, Leiva DR, Deledda S, Hauback BC, Botta WJ. Cold rolling of MgH_2 powders containing different additives. Int J Hydrogen Energy 2013;36:16193–8. https://doi.org/10.1016/j.ijhydene.2013.10.029.
[20] Leiva DR, Fruchart D, Bacia M, Girard G, Skryabina N, Villela ACS, et al. Mg alloy for hydrogen storage processed by SPD. Int J Mater Res 2009;100:1739–47.
[21] Leiva DR, Jorge Junior AM, Ishikawa TT, Huot J, Fruchart D, Miraglia S, et al. Nanoscale grain refinement and H-sorption properties of MgH_2 processed by high-pressure torsion and other mechanical routes. Adv Eng Mater 2010;12:786–92.
[22] Jorge Junior AM, Prokofiev E, Ferreira de Lima G, Rauch E, Veron M, Botta WJ, et al. An investigation of hydrogen storage in a magnesium-based alloy processed by equal channel angular pressing. Int J Hydrogen Energy 2013;38:8306–12.
[23] Soyama J, Martins Triques MR, Leiva DR, Jorge Junior AM, Pereira da Silva E, Pinto HC, et al. Hydrogen storage in heavily deformed ZK60 alloy modified with 2.5 wt% Mm addition. Int J Hydrogen Energy 2016;41:4177–84.
[24] Asselli AAC, Leiva DR, Huot J, Kawasaki M, Langdon TG, Botta WJ. Effects of equal-channel angular pressing and accumulative roll-bonding on hydrogen storage properties of a commercial ZK60 magnesium alloy. Int J Hydrogen Energy 2015;40:16971–6. https://doi.org/10.1016/j.ijhydene.2015.05.149.
[25] Jorge Junior AM, Ferreira de Lima G, Martins Triques MR, Botta WJ, Kiminami CS, Nogueira RP, et al. Correlation between hydrogen storage properties and textures induced in magnesium through ECAP and cold rolling. Int J Hydrogen Energy 2014;39:3810–21.
[26] Leiva DR, Costa HCA, Huot J, Pinheiro TS, Jorge Junior AM, Ishikawa TT, et al. Magnesium-nickel alloy for hydrogen storage produced by melt spinning followed by cold rolling. Mater Res 2012;15(5):813–7.
[27] Soyama J, Floriano R, Leiva DR, Guo Y, Jorge Junior AM, Silva EP, et al. Severely deformed ZK60 + 2.5% Mm alloy for hydrogen storage produced by two different processing routes. Int J Hydrogen Energy 2016;41:11284–92. https://doi.org/10.1016/j.ijhydene.2016.05.031.
[28] Grill A, Horky J, Panigrahi A, Krexner G, Zehetbauer M. Long-term hydrogen storage in Mg and ZK60 after severe plastic deformation. Int J Hydrogen Energy 2015;40:17144–52. https://doi.org/10.1016/j.ijhydene.2015.05.145.
[29] Asselli AAC, Hébert NB, Huot J. The role of morphology and severe plastic deformation on the hydrogen storage properties

of magnesium. Int J Hydrogen Energy 2014;39:12778–83. https://doi.org/10.1016/j.ijhydene.2014.06.042.
[30] Hongo T, Edalati K, Arita M, Matsuda J, Akiba E, Horita Z. Significance of grain boundaries and stacking faults on hydrogen storage properties of Mg_2Ni intermetallics processed by high-pressure torsion. Acta Mater 2015;92:46–54.
[31] Dupasquier A, Mills Jr AP. Positron spectroscopy of solids. Amsterdam: North-Holland; 1995.
[32] Banhart J, Lay MDH, Chang CST, Hill AJ. Kinetics of natural aging in Al–Mg–Si alloys studied by positron annihilation lifetime spectroscopy. Phys Rev B 2011;83:014101.
[33] Eddahbi M, Pérez P, Monge MA, Garcés G, Pareja R, Adeva P. Microstructural characterization of an extruded Mg–Ni–Y–RE alloy processed by equal channel angular extrusion. J Alloys Compd 2009;473:79–86. https://doi.org/10.1016/j.jallcom.2008.05.064.
[34] Zou B, Chen ZQ, Liu CH, Chen JH. Vacancy–Mg complexes and their evolution in early stages of aging of Al–Mg based alloys. Appl Surf Sci 2014;298:50–5.
[35] Ortega Y, Del Río J. Detection of $Mg_{17}Al_{12}$ precipitates in deformed thermal-aged AZ91 alloy by positron annihilation spectroscopy. Phys Status Solidi 2004;3:471–5. https://doi.org/10.1002/pssa.200306745.
[36] Kirkegaard P, Pedersen NJ, Eldrup MM. PATFIT-88: a data-processing system for positron annihilation spectra on mainframe and personal computers. Risø-M; No. 2740. 1989.
[37] Jing-yuan LI, Jian-xin XIE, Jun-bing JIN, Zhi-xiang WANG. Microstructural evolution of AZ91 magnesium alloy during extrusion and heat treatment. Trans Nonferrous Metals Soc China 2012;22:1028–34. https://doi.org/10.1016/S1003-6326(11)61279-X.
[38] Jabbari-Taleghani MA, Torralba JM. Hot workability of nanocrystalline AZ91 magnesium alloy. J Alloys Compd 2014;595:1–7. https://doi.org/10.1016/j.jallcom.2014.01.091.
[39] Léon A, Knystautas EJ, Huot J, Schulz R. Hydrogenation characteristics of air-exposed magnesium films. J Alloys Compd 2002;345:158–66. https://doi.org/10.1016/S0925-8388(02)00394-8.
[40] Yao HB, Li Y, Wee ATS. An XPS investigation of the oxidation/corrosion of melt-spun Mg. Appl Surf Sci 2000;158:112–9. https://doi.org/10.1016/S0169-4332(99)00593-0.
[41] Liu M, Zanna S, Ardelean H, Frateur I, Schmutz P, Song G, et al. A first quantitative XPS study of the surface films formed, by exposure to water, on Mg and on the Mg–Al intermetallics: Al_3Mg_2 and $Mg_{17}Al_{12}$. Corros Sci 2009;51:1115–27. https://doi.org/10.1016/j.corsci.2009.02.017.
[42] Santamaria M, Di Quarto F, Zanna S, Marcus P. Initial surface film on magnesium metal: a characterization by X-ray photoelectron spectroscopy (XPS) and photocurrent spectroscopy (PCS). Electrochim Acta 2007;53:1314–24.
[43] Vincent SD, Huot J. Effect of air contamination on ball milling and cold rolling of magnesium hydride. J Alloys Compd 2011;509:L175–9.
[44] Lang J, Skryabina N, Fruchart D, Danaie M, Huot J. Microstructure of cold rolled magnesium and magnesium hydrides for hydrogen storage applications. Chem Sustain Dev 2013;21:1–8.

Please cite this article in press as: Floriano R, et al., Low temperature rolling of AZ91 alloy for hydrogen storage, International Journal of Hydrogen Energy (2017), https://doi.org/10.1016/j.ijhydene.2017.10.035